

Using failed supernovae to constrain the Galactic r-process element production

B. Wehmeyer,^{1,6★} C. Fröhlich^{1,6}, B. Côté,^{2,6,7} M. Pignatari^{2,3,6,7}
and F.-K. Thielemann^{4,5}

¹Department of Physics, North Carolina State University, 2401 Stinson Dr, Raleigh, NC 27695-8202, USA

²Konkoly Observatory, Research Centre for Astronomy and Earth Sciences, Hungarian Academy of Sciences, Konkoly-Thege Miklós út 15-17, H-1121 Budapest, Hungary

³E.A. Milne Centre for Astrophysics, Department of Physics & Mathematics, University of Hull, Hull HU6 7RX, UK

⁴University of Basel, Department of Physics, Klingelbergstr. 82, CH-4056 Basel, Switzerland

⁵GSI Helmholtzzentrum für Schwerionenforschung, Planckstraße 1, D-64291 Darmstadt, Germany

⁶Joint Institute for Nuclear Astrophysics – Center for the Evolution of the Elements

⁷NuGrid collaborations, <http://nugridstars.org>

Accepted 2019 May 5. Received 2019 April 18; in original form 2018 December 31

ABSTRACT

Rapid neutron capture process (r-process) elements have been detected in a large fraction of metal-poor halo stars, with abundances relative to iron (Fe) that vary by over two orders of magnitude. This scatter is reduced to less than a factor of 3 in younger Galactic disc stars. The large scatter of r-process elements in the early Galaxy suggests that the r-process is made by rare events, like compact binary mergers and rare sub-classes of supernovae. Although being rare, neutron star mergers alone have difficulties to explain the observed enhancement of r-process elements in the lowest metallicity stars compared to Fe. The supernovae producing the two neutron stars already provide a substantial Fe abundance where the r-process ejecta from the merger would be injected. In this work we investigate another complementary scenario, where the r-process occurs in neutron star-black hole mergers in addition to neutron star mergers. Neutron star-black hole mergers would eject similar amounts of r-process matter as neutron star mergers, but only the neutron star progenitor would have produced Fe. Furthermore, a reduced efficiency of Fe production from single stars significantly alters the age–metallicity relation, which shifts the onset of r-process production to lower metallicities. We use the high-resolution [(20 pc)³/cell] inhomogeneous chemical evolution tool ‘ICE’ to study the outcomes of these effects. In our simulations, an adequate combination of neutron star mergers and neutron star-black hole mergers qualitatively reproduces the observed r-process abundances in the Galaxy.

Key words: Galaxy: abundances – Galaxy: evolution – nuclear reactions, nucleosynthesis, abundances – Supernovae: general.

1 INTRODUCTION

The r-process (see e.g. Cowan et al. 1991; Arnould, Goriely & Takahashi 2007; Thielemann et al. 2011; Cowan et al. 2019, and references therein) is one of the dominant sources of elements heavier than Fe. At present, it is still unclear whether neutron star mergers (NSMs, since recently the only observed and confirmed r-process site) are the *exclusive* site of this process (e.g. Cescutti et al. 2015; Hirai et al. 2015; Ishimaru, Wanajo & Prantzos 2015; Shen et al. 2015; van de Voort et al. 2015; Wehmeyer, Pignatari &

Thielemann 2015; Thielemann et al. 2017; Côté et al. 2018; Hotokezaka, Beniamini & Piran 2018; Ojima et al. 2018; Siegel, Barnes & Metzger 2018; Cowan et al. 2019; Haynes & Kobayashi 2019). While early scientific studies argued that neutrino fluxes in core-collapse supernovae (CCSNe) would have the right properties to host neutrino-driven nucleosynthesis (see e.g. Arcones & Thielemann 2013 and references therein) that might include the r-process (e.g. Takahashi, Witt & Janka 1994; Woosley et al. 1994), later and more advanced calculations (e.g. Liebendörfer et al. 2003) pointed to proton-rich conditions in their innermost ejecta, rather causing a *vp* process (Fröhlich et al. 2006a,b; Pruet et al. 2005, 2006; Wanajo 2006, 2013) instead of the r-process. However, the collapse of the core of a massive star leads either to a CCSN and a neutron star (NS)

* E-mail: bwehmey@ncsu.edu

or to the formation of a black hole (BH; e.g. Heger et al. 2003). When two NSs merge (e.g. Lattimer & Schramm 1974; Paczynski 1986; Eichler et al. 1989, but see also more recent works, e.g. Rosswog et al. 2018), conditions for the onset of the r-process are met (Freiburghaus, Rosswog & Thielemann 1999; Panov, Korneev & Thielemann 2008; Korobkin et al. 2012; Bauswein, Goriely & Janka 2013; Rosswog 2013; Rosswog et al. 2014; Wanajo et al. 2014; Eichler et al. 2015; Just et al. 2015). This site has been confirmed by gravitational wave detection GW170817 (e.g. Abbott et al. 2017a), followed by its optical counterpart, kilonova SSS17a, showing evidence of the successful production of r-process elements (e.g. Abbott et al. 2017b,c). Hence, NSMs are a confirmed source of Galactic r-process elements. Considering this site as *the exclusive* r-process site, however, comes with two distinct issues:

(i) *r-process elements are abundant already at very low metallicities*. Two CCSNe must have occurred before the NSM event in order to produce the two involved NSs. Hence, the interstellar medium (ISM) hosting the NSM is already polluted by the Fe-rich ejecta of those two CCSNe. Many stars with low metallicity already show high r-process abundances compared to Fe, up to two orders of magnitude larger than solar (e.g. Sneden, Cowan & Gallino 2008; Roederer et al. 2010; Hansen et al. 2018). Such enhancements are difficult to explain by a scenario where NSMs act as *the exclusive* r-process element production source (e.g. Argast et al. 2004; Wehmeyer et al. 2015).

(ii) *r-process elemental abundances in low metallicity stars show a large scatter in comparison to solar metallicity stars*. The observed abundance scatter in alpha elements¹ with respect to Fe remains rather small throughout the entire chemical evolution. Instead, r-process elements show a much larger scatter in abundances at low metallicities (Roederer et al. 2010; Beers et al. 2018). Since alpha elements are made mostly by CCSNe, this suggests that r-process elemental production events should occur at a lower frequency than CCSNe (e.g. Thielemann 2015, Thielemann et al. 2017).

Recent works to address these open questions have mostly considered two scenarios, i.e. adding a rare sub-class of supernova as second early r-process site, or considering sub-haloes of the Galaxy as independent building blocks that will later merge to form the Galaxy. The former approach is based on the assumption that there could be a second, rare r-process production site, e.g. (the sub-class of) magnetorotationally driven supernovae (or ‘jet-supernovae’, see e.g. Winteler et al. 2012; Mösta et al. 2015; Nishimura et al. 2017; Halevi & Mösta 2018). Since this site would eject r-process elements and negligible amounts of Fe, r-process elements could be released into a region of lower metal content than a NSM could (those require two NSs to be present and thus two previous supernovae, already enhancing the ISM with metals), if the occurrence rate of such a supernova would be low (as expected due to the required high magnetic fields) in comparison to ‘regular’ CCSNe. Stars being polluted by such an event would inherit high r-process abundances in comparison to stars polluted by regular CCSNe. This would also allow to explain the large scatter seen in r-process abundances in low metallicity stars.

These considerations were already discussed in Cescutti et al. (2015) and Wehmeyer et al. (2015). However, despite the fact that 10^{15} Gauss NSs as remnants of this distinct supernova channels have

been detected, this scenario still has to wait for an observational confirmation (Fujimoto et al. 2006; Fujimoto, Nishimura & Hashimoto 2008; Winteler et al. 2012; Mösta et al. 2014). Furthermore, this nucleosynthesis site involves the difficulty of high-resolution treatments of the magnetorotational instability (e.g. Mösta et al. 2015; Rembiasz et al. 2016; Sawai & Yamada 2016; Nishimura et al. 2017; Obergaulinger, Just & Aloy 2018).

A second approach to solve the difficulties (i) and (ii) above is to consider dwarf galaxies as individually developing sub-systems that will merge to later form the Galactic halo (e.g. Hirai et al. 2015). Observations of dwarf galaxy systems show that these systems have lower star formation efficiency (Kirby et al. 2013) and higher gas outflow rates (see predictions from cosmological simulations, e.g. Muratov et al. 2015; Pillepich et al. 2018). These features allow the contribution of NSMs to already take place at low metallicities (because lower star formation efficiency slows down the temporal evolution of [Fe/H], which allows NSMs to appear at lower [Fe/H] values with respect to the star formation rate, cf. Ishimaru et al. 2015) and provide large abundance scatter (among others, because of gas outflows in chemodynamical models, cf. Hirai et al. 2015, and the stochastic nature of dwarf systems, cf. Ojima et al. 2018). Although such systems are observationally confirmed to have seen r-process production events (Ji et al. 2016; Marshall et al. 2018), it is yet unclear whether a stochastic chemical evolution model featuring low star formation efficiencies is applicable to the bulk of these kind of systems (Kirby et al. 2013; Ojima et al. 2018).

In this paper, we study an alternative scenario with respect to the ones discussed above: We consider BH–NS mergers (BHNSM) as second r-process elemental production site in addition to NSMs. This site has one major difference compared to NSMs: BHNSM require only *one* NS to be present in the system. This means that only *one* CCSN is required in the system before the r-process event. This allows BHNSMs to occur at lower initial metallicities than NSMs. Also, the slower overall increase of metallicity due to less successful CCSNe permits the presence of r-process rich stars at lower metallicities.

This work is organized as follows. In Section 2, we discuss the astronomical observations relevant for this work. In Section 3, we introduce the model used to compute the evolution of abundances. In Section 4, we present the influence of the different r- and non-r-process sites on the evolution. In Section 5, our results are summarized and discussed.

2 OBSERVATIONS

2.1 Europium as tracer of r-process elements

Galactic chemical evolution (GCE) is a powerful tool to study the contributions of the different elemental production sites to stellar abundances. For many lighter elements (e.g. Mg, O, C), the production sites are well known. Beyond Fe, the r-process contributions provide about half of the element abundances in the Solar system, and are the dominant source in the Universe of several elements like Ir, Pt, and Au (for a recent review, see Cowan et al. 2019). Eu is the most observed r-process element, and it is used as a diagnostic to study the history of the r-process enrichment of the Galaxy (e.g. Burris et al. 2000). Eu abundances are derived using mostly the two ultraviolet lines at 4192.70 and 4205.05 Å (e.g. Biémont et al. 1982).

We make use of the abundance database SAGA (Stellar Abundances for Galactic Archaeology, e.g. Suda et al. 2008, 2011;

¹Among the stable alpha elements are C, O, Ne, Mg, Si, S, Ar, and Ca.

Yamada et al. 2013), with $[\text{Eu}/\text{Fe}]^2$ abundances mainly from Francois et al. (2007), Simmerer et al. (2004), Barklem et al. (2005), Roederer et al. (2010, 2014a,b,c), Shetrone, Côté & Stetson (2001), Shetrone et al. (2003), Geisler et al. (2005), Cohen & Huang (2009), Letarte et al. (2010), Starkenburg et al. (2013), and McWilliam, Wallerstein & Mottini (2013). We exclude carbon-enhanced metal-poor (‘CEMP’) stars, i.e. stars with $[\text{C}/\text{Fe}] \geq 1$ and $[\text{Fe}/\text{H}] \leq -1$ and stars with binary nature, since the surface abundances of such objects are expected to be affected by pollution from a binary companion (Ryan et al. 2005), which is beyond the scope of this study. When comparing the observed Eu abundances as a function of $[\text{Fe}/\text{H}]$ with those of lighter alpha elements (primarily those made by CCSNe), it is very striking to see that the two curves behave similarly close to solar metallicities, but differ greatly at low metallicities (e.g. Thielemann et al. 2017; Cowan et al. 2019), making metal-poor stars to unique tracers of the early evolution of Galactic *r*-process nucleosynthesis (e.g. Sneden et al. 2008; Frebel 2018; Horowitz et al. 2018).

2.2 GW170817/SSS17a

The detection of the gravitational wave event GW170817 (e.g. Abbott et al. 2017a) has been interpreted as a coalescence of two compact objects with masses in the range $1.17 M_{\odot} \leq m \leq 1.60 M_{\odot}$. The GW emission was followed by the detection of a kilonova (SSS17a) whose light curve suggests *r*-process element production (e.g. Chornock et al. 2017; Cowperthwaite et al. 2017; Tanaka et al. 2017; Villar et al. 2017). Lanthanides as Eu were produced in the event (e.g. Tanvir et al. 2017; Wollaeger et al. 2018). While the majority of the literature suggests that the coalescence of two NSs was the origin of this astronomical event (Abbott et al. 2018a), it cannot be ruled out that the event was actually the coalescence of a NS and a BH (Hinderer et al. 2018). Furthermore, Hinderer et al. (2018) showed that the *GW only* and the *electromagnetic only* observations can only rule out a BHNSM for an extreme range of the parameter space and find that 40 percent of the parameter space set by the nuclear and astrophysical uncertainties would permit a BHNSM event instead of a NSM event in the case of GW170817/SSS17a. A possible formation channel for a required stellar mass BH – considered in this study – is that it originates in a failed SN (e.g. Heger et al. 2003), which will be discussed in Sections 3.2.3 and 3.2.4. Another possible origin of the required stellar mass BH is e.g. in primordial fluctuations in the early Universe. A probable formation channel of such objects is described in e.g. Garcia-Bellido, Linde & Wands (1996), Carr, Kühnel & Sandstad (2016), and Garcia-Bellido (2018). However, their occurrence frequency in BHNSMs is hard to predict; therefore, we do not include them here explicitly.

3 THE GCE MODEL

In comparison to homogeneous GCE models, inhomogeneous models track the *location* of the nucleosynthesis sites. This permits to reproduce the *scatter* of abundances instead of predicting a linear evolution. On the other hand, large-scale effects (e.g. galaxy collisions, spiral arms mixing) can only be approximated in such models. In this study we use the inhomogeneous chemical evolution model described in Wehmeyer et al. (2015). In the following sections, we recall the main components of the model

Table 1. Main infall parameters. See Wehmeyer et al. (2015) for details on the parameters.

Parameter	Description	Value
M_{tot}	Total infall mass	$10^8 M_{\odot}$
τ	Time scale of infall decline	$5 \times 10^9 \text{ y}$
t_{max}	Time of the highest infall rate	$2 \times 10^9 \text{ y}$
t_{final}	Duration of the simulation	$13.6 \times 10^9 \text{ y}$

for convenience (Sections 3.1, 3.2.1, and 3.2.2) and highlight the improvements made to the model for the purpose of this study, especially the treatment of the additional *r*-process site related to BHNSMs (Sections 3.2.3 and 3.2.4).

3.1 General set-up

We set up a cube of $(2 \text{ kpc})^3$ in the Galaxy that is cut into 100^3 sub-cubes with an edge length of 20 pc. During each time step of 1 My, the following calculations are performed:

(i) Primordial matter is assumed to fall uniformly into each simulation sub-cube. The total amount of gas falling into the simulation volume is calculated via a

$$\dot{M}(t) = at^b e^{-t/\tau}, \quad (1)$$

prescription, which permits two main infall components: An initial constant rise of infall following by an exponential decay of the infall rate. While τ and the total Galaxy evolution time t_{final} are fixed initially, the parameters a and b can be determined alternatively from M_{tot} (the total infall mass integrated over time), defined by

$$M_{\text{tot}} = \int_0^{t_{\text{final}}} at^b e^{-t/\tau} dt, \quad (2)$$

and the time of maximal infall t_{max} , given by

$$t_{\text{max}} = b\tau. \quad (3)$$

See Table 1 for the applied parameters.

(ii) The total gas mass in the volume is calculated and star formation is triggered. We use a Schmidt law with a density power $\alpha = 1.5$ (since we aim star formation to be triggered by both the density of the ISM and cloud–cloud interactions; see Schmidt 1959; Larson 1991; Kennicutt 1998) to determine total mass of stars that are born in the current time step. This number is then divided by the integrated initial mass function (‘IMF’, Salpeter type with a slope of -2.35) to obtain the number of stars formed per time step.

(iii) Once the number of newly born stars is calculated, star-forming cells are selected randomly. Since star formation can be triggered by events as cloud–cloud interactions (e.g. shells of supernova remnants), we prefer cells with higher densities as location for newly born stars.

(iv) Once a star-forming cell is selected, we choose the mass of the newly born star randomly, with mass probabilities obeying a Salpeter type IMF with a slope of -2.35 , in the mass range of $0.1 M_{\odot} \leq m \leq 50 M_{\odot}$.³ In order to permit stellar masses to be well distributed (i.e. no bottom heavy IMF), we permit star formation only in cells containing at least $50 M_{\odot}$ of gas. We consider stars with birth masses below $8 M_{\odot}$ as low and intermediate mass stars (LIMSS), and stars more massive than $8 M_{\odot}$ as high mass stars (HMSs).

³In this manuscript - when referring to stellar masses (excluding NSs and BHs) - we refer to the zero-age main-sequence mass of the star.

²We use the notation $[A/B] = \log(A/B)_{\text{star}} - \log(A/B)_{\odot}$

(v) The newly born star inherits the composition of the ISM out of which it is formed. From its birth mass and metallicity, we obtain its life expectation using the Geneva Stellar Evolution and Nucleosynthesis Group (cf. Schaller et al. 1992; Charbonnel et al. 1993; Schaerer et al. 1993a,b) predictions, given by

$$\log(t) = (3.79 + 0.24Z) - (3.10 + 0.35Z)\log(M) \\ + (0.74 + 0.11Z)\log^2(M), \quad (4)$$

where t is the expected lifetime of a star in My, Z is the metallicity with respect to solar, and M the star's mass in solar masses.

(vi) Once a star has reached the end of its calculated lifetime, a stellar death event is triggered (according to its birth mass), as discussed below.

3.2 Nucleosynthesis sites

3.2.1 Low and intermediate mass stars

LIMs produce most of C and N in the Galactic disc (e.g. Kobayashi & Nakasato 2011). During the Asymptotic Giant Branch phase, LIMs produce the bulk of the slow neutron capture ('s-process') abundances beyond Sr present in the Solar system (see e.g. Käppeler et al. 2011; Bisterzo et al. 2014, and references therein). LIMs do not make significant contributions to the Galactic Fe or Eu inventory. Therefore, we only consider them as objects locking up gas for the duration of their lifetime for the purpose of our simulation. LIMs return a significant amount of H and He in the ISM, marginally affecting the [Fe/H] ratios in the ISM. However, results and conclusions presented in this work are not affected. Once dying, LIMs give back portions of their locked-up gas via stellar winds (resulting in a planetary nebula), leaving behind a white dwarf. Since planetary nebulae have observed sizes of a few tenths of to a few light years (e.g. Cat's eye nebula NGC 6543 with a 0.2 light-year diameter, Reed et al. 1999; Helix nebula with 2.87 light years, O'Dell, McCullough & Meixner 2004), for the purpose of our simulation, we simply return the locked-up mass to the local cell once an LIM has reached the end of its lifetime.

3.2.2 Thermonuclear supernovae

Since many stars in the Galaxy are born in double-star systems (e.g. Duchêne & Kraus 2013), there is a chance that a newly born star has a companion that meets the prerequisites to let the double-star system later undergo a supernova event of type Ia (SNIa). We follow the analytical suggestion of Greggio (2005) to simplify all associated stellar and binary evolution aspects to one probability ($P_{\text{SNIa}} = 9 \times 10^{-4}$) for a newly born intermediate mass star (IMS, stars with masses in the range $1 M_{\odot} \leq m \leq 10 M_{\odot}$) to be born in a system that will later end up as an SNIa. This is equivalent to a rate of 7.49×10^{-4} SNIa events per unit solar mass of stars formed. At the end of the lifetime of the second IMS, we inject 10^{51} erg of energy at the location of the event and emit the event specific yields (cf. Iwamoto et al. 1999, model CDD2). As in Wehmeyer et al. (2015), we simply eject the same amount of Fe at all metallicities. This might be unrealistic (e.g. Timmes, Brown & Truran 2003; Thielemann et al. 2004; Travaglio, Hillebrandt & Reinecke 2005; Bravo et al. 2010; Seitzzahl et al. 2013; Leung & Nomoto 2018), but this approximation does not strongly affect the outcomes of our simulation. SNIa do not contribute to the r-process production, but they are the dominant source of Fe in the Galactic disc (e.g. Matteucci & Greggio 1986). Therefore, we need to take into account

the SNIa contribution to reproduce the chemical evolution of the [Eu/Fe] ratio in the Galaxy.

3.2.3 Core collapse supernovae and failed supernovae

Stars more massive than $10 M_{\odot}$ will experience all evolutionary stages until Si burning and the formation of an Fe core (e.g. Jones et al. 2013). With the loss of its central energy source, the star cannot withstand the gravitational inward pull anymore and collapses. The core is compressed until it reaches nuclear densities, a so-called proto-NS. Neutrinos originating from the proto-NS lead to neutrino and anti-neutrino capture on neutrons and protons, which heat up matter in the so-called gain region (e.g. Burrows 2013; Janka, Melson & Summa 2016; Janka 2017; Burrows et al. 2018) and lead to a successful explosion if the deposited energy is sufficient. This is the case for a large fraction of initial stellar masses beyond $10 M_{\odot}$, but dependent on the stellar structure/compactness inherited from the pre-collapse stellar evolution this mechanism fails and results in the formation of a BH (e.g. Heger et al. 2003). In order to be able to determine when a star fails to explode instead of ending up in a supernova, the explosion energy predictions of the CCSN simulation suite PUSH (Perego et al. 2015; Curtis et al. 2019; Ebinger et al. 2019) are used to understand under which conditions massive stars collapse to a BH instead of exploding in a CCSN and leaving behind a NS. Their conclusions are that stars in the mass region $22.8 M_{\odot} \leq m \leq 25.6 M_{\odot}$ (at $Z = Z_{\odot}$) do not have sufficient explosion energies to withstand the gravitational collapse. These stars failing to explode in the CCSN simulations are considered in the GCE suite in the following way: they collapse to a BH, without ejecting Fe. Since most massive stars have at least one companion (e.g. Duchêne & Kraus 2013), we then use these results to constrain the BHNSM rate and the implications of this *second* r-process site on the chemical evolution of the Galaxy (see Section 3.2.4 for a detailed discussion of the implementation of BHNSMs/NSMs).

While we *do* have prescriptions for the explodability and thus the production of metals by HMSs at the end of their lifetime for solar metallicity HMSs, it is expected that for low metallicities, in contrast to solar metallicities, a larger fraction of massive stars ends as BHs rather than CCSNe, due to smaller opacities and smaller amounts of mass loss during the hydrostatic phase. Therefore, we employ the predictions made by these studies only close to solar metallicities and make different assumptions for lower metallicity HMSs: Since the explodability tends to scale with the progenitor compactness (Ebinger 2017; Curtis et al. 2019; Ebinger et al. 2019; Ebinger et al. in preparation), we employ the compactness of low metallicity progenitors at the time of the onset of the gravitational collapse as indicator whether the individual low metallicity progenitors will later undergo a successful CCSN. Lower opacity due to less metal content leads to less radiation scatter in the outer layers of lower metallicity stars. This stellar wind loss has an effect on the compactness of stars: It leaves lower metallicity stellar cores at a higher compactness in comparison to their solar metallicity counterparts. Since the explosion calculations within the PUSH model have not yet been completed for lower metallicities, we utilize a simplified concept: In addition to the known explodability of solar metallicity HMSs, we test three extreme cases: all stars $\geq 20 M_{\odot}$ ($\geq 25 M_{\odot}$, $\geq 30 M_{\odot}$) at metallicities $Z \leq 10^{-2} Z_{\odot}$ (chosen to be metallicity-wise in between the current (Curtis et al. 2019; Ebinger et al. 2019) predictions at Solar metallicity, and Ebinger et al. (in preparation, predictions for [Fe/H] = -4) are doomed to die in a

failed SN at the end of their lifetime. This permits to account for the extent of the effects of the stellar wind mass losses, and therefore for the varied compactness of a lower metallicity HMS.

3.2.4 NSM and BHNSM

If a double-star system consists of two HMSs, both end their life in either a failed or successful supernova (e.g. Nomoto, Kobayashi & Tominaga 2013). If the two remaining objects (two NSs in the case of two successful CCSNe, two BHs in the case of two failed SNe, and one NS and one BH in the case of one successful CCSN and one failed SN) survive the supernova kicks and remain gravitationally bound (e.g. Tauris et al. 2017), this bound system emits gravitational waves and merges later. In this case, a compact binary merger (CBM, either a NSM or a BHNSM) event occurs. BHNSMs can be an important source of *r*-process material. Korobkin et al. (2012) give results for the merger of a $1.4 M_{\odot}$ NS with either a $5 M_{\odot}$ or a $10 M_{\odot}$ BH, which produce comparable yield curves and ejecta masses to NSMs. NSMs, on the other hand, require two NSs and thus two successful CCSNe before the CBM event, so the surrounding ISM is already polluted with the ejecta of these two CCSNe and thus already enriched in metals. This means that the CBM products are ejected into a region where the metallicity is already high in comparison to the case of a BHNSM, where only *one* NS is required, which means that only *one* CCSN polluted the ISM with metals.⁴ Theoretical predictions for NSM rates vary strongly (e.g. Kalogera et al. 2004), while the rates for BHNSMs are very controversial (e.g. Mennekens & Vanbeveren 2014). Also, different nucleosynthesis (e.g. Abbott et al. 2017a; Chornock et al. 2017; Cowperthwaite et al. 2017; Kasen et al. 2017; Tanaka et al. 2017; Wang et al. 2017; Gompertz et al. 2018; Hotokezaka et al. 2018; Rosswog et al. 2018) and GCE studies (e.g. Matteucci et al. 2014; Cescutti et al. 2015; Hirai et al. 2015; Ishimaru et al. 2015; Shen et al. 2015; Wehmeyer et al. 2015; Komiya & Shigeyama 2016; Haynes & Kobayashi 2019) use different rates for this kind of event. Côté et al. (2017) have compiled several modern GCE calculations involving NSM event probabilities and found that the rate assumptions differ by two orders of magnitude from study to study. This fact originates – among others – in the different treatment of infall prescriptions, differences in star-forming prescription, employed IMF, CCSN/SNIa ejecta, and total ejected mass per NSM. When the assumptions in these studies are normalized to the same IMF, Fe yields, and Eu yields, then the number of NSMs per unit of stellar mass formed found in different studies converges within a factor of 4 (see Côté et al. 2017). While these theoretical prescriptions for NSM per unit volume or unit stellar mass formed vary greatly, a new approach helps us to determine the actual rate of CBMs in the local Universe: the detection of gravitational waves. While the first detections were attributed to BH–BH mergers (and are thus of less importance for this study) more recent ones have detected a NSM event (e.g. Abbott et al. 2018a,b, which predict a NSM rate of $1540_{-1220}^{+3200} \text{ Gpc}^{-3} \text{ yr}^{-1}$). In order to reduce the number of free parameters in the formation channel, we use a simpler approach: We use an *effective* probability factor $P_{\text{r-roc}}$, which represents the probability for a newly born HMS to be in a system that will end up as a NSM/BHNSM, producing the *r*-process. We use $P_{\text{r-roc}} = 4$ per cent, which translates to (assuming

⁴Following this argumentation, BH–BH mergers might occur in a region where *no* CCSN has occurred and is thus metal-free. However, since BH–BH mergers do not eject any *r*-process enriched material, we do not consider this case here.

a Salpeter initial mass function with a slope of -1.35 , and a standard Cosmic star formation history with constant CBM delay times; see Côté et al. 2017 for the details of this conversion) 1.03×10^{-4} CBM events per unit solar mass of stars formed. This rate is arguably high (see above and Côté et al. 2017 for a rate comparison of recent GCE models), but would correspond to an event rate of $\approx 1800 \text{ Gpc}^{-3} \text{ yr}^{-1}$, which is well within the rate predicted by LIGO/Virgo.

However, this approach has one major caveat: If the BH in the binary system is too massive (or does not have sufficient angular momentum), this will lead to the NS either being swalled without disruption or being disrupted and forming a disc, but inside the last stable orbit, i.e. not leading to mass ejection. The upper limit for BH masses to permit ejecta depends on the NS equation of state, the BH mass, and the BH spin (e.g. Belczynski et al. 2017). With present knowledge (see Rosswog 2015), an upper limit seems to be in the range of $10\text{--}14 M_{\odot}$ for the BH mass. Consequently, it is important how massive the resulting BHs would be after a star has undergone a failed SN. Two points need to be considered: (a) the mass loss during stellar evolution and (b) which part of the pre-collapse star ends up in the BH and which part is still ejected in a failed SN. Possible options are that at least the H-envelope or all matter outside the CO core (or even more) is ejected. Looking at tables and figures in Thielemann et al. (2018) and Ebinger et al. (2019), referring to stellar models from Hirschi (2007), Limongi & Chieffi (2006a,b) – and Woosley, Heger & Weaver (2002), Woosley & Heger (2007), respectively – with different rotation rates and metallicities, it turns out that for high (but credible, e.g. Hirschi, Meynet & Maeder 2005) rotation rates a $30 M_{\odot}$ star can lose half of its mass and an $80 M_{\odot}$ star can even end in a final pre-collapse mass of $20 M_{\odot}$. Including also the most recent results of Limongi & Chieffi (2018), we find He-core masses below the above-mentioned upper mass limit (for the disruption of the NS by the BH under ejection of *r*-process matter) for stars with initial masses below $25\text{--}30 M_{\odot}$, and CO-masses below these limits up to initial masses of $40 M_{\odot}$. Thus, while a point of caution should be kept in mind regarding the BHNSM scenario, it will clearly not be excluded. The occurrence rates utilized here should, however, be taken as an upper limit.

4 RESULTS

4.1 CBMs may explain *r*-process element GCE

Using our model, we study the effect of using BHNSMs as additional *r*-process production site. Our results suggest that the discussed deficiencies of using NSMs as exclusive *r*-process element production site can be cured by adding this second site. As can be seen in Fig. 1, both challenges mentioned in the Introduction section can be solved by using our model and including BHNSMs. Model stars (red, green, and blue squares) are

- (i) abundant in a very low metallicity region,
- (ii) show a large abundance scatter at lower metallicities, while this scatter is reduced towards higher metallicities, and
- (iii) are in qualitative agreement with the observations (magenta crosses).

This can be explained in the following way: Regarding point

- (i) BHNSMs require only *one* previous CCSN event (since they only require *one* NS before the *r*-process event as opposed to *two* previous CCSNe for NSM). This implies that this *r*-process event potentially happens at lower metallicities compared to NSM. See also Section 3.2.4 for discussion, and Fig. 2 for illustration.

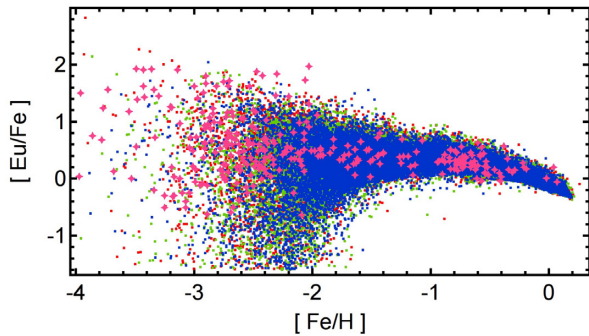


Figure 1. Effect of the different choices of the prescriptions for failed SN at low metallicities on the GCE of [Eu/Fe]: Magenta crosses represent observations. Red (green, blue) squares represent GCE models where all stars $\geq 20 M_{\odot}$ ($\geq 25 M_{\odot}$, $\geq 30 M_{\odot}$) at metallicities $Z \leq 10^{-2} Z_{\odot}$ are forming failed SNe at the end of their life.

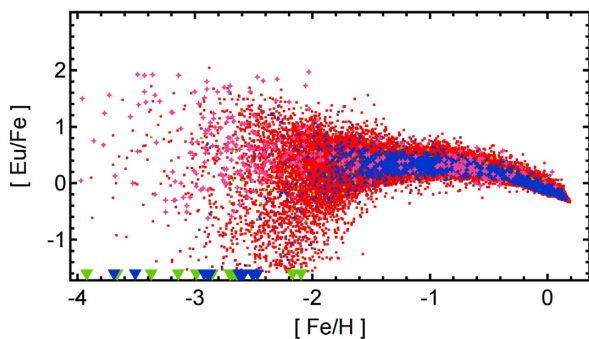


Figure 2. Locations of NSM/BHNSM events in the [Eu/Fe] versus [Fe/H] space of our fiducial model (failed SNe for $m \geq 30 M_{\odot}$ at metallicity lower than $Z \leq 10^{-2} Z_{\odot}$). Magenta crosses represent observations. Red squares represent all model stars. Green and blue squares are the locations where BHNSMs or NSMs occur, respectively. This allows us to determine at what point the different r-process events contribute to the Galactic r-process element inventory. Note that the first r-process events always have to occur in an r-process element free/poor environment, and thus are located at or near $[\text{Eu}/\text{Fe}] = -\infty$. We put green and blue triangles at the [Fe/H] locations above where the first BHNSM or NSM occurs.

Additionally, another effect is relevant here: A model where a certain amount of stars fail to explode in a CCSN (and thus do not contribute to the Fe inventory of the Galaxy) slows down the [Fe/H] enrichment over time, compared to a model where every star succeeds to explode and thus contributes to the Fe evolution. This reduces the number of CCSNe per time step. See Section 4.2 for discussion.

(ii) Since BHNSMs can occur while ejecting less Fe per r-process event (as discussed above), their event specific [Eu/Fe] (including the previous CCSN) is a factor of 2 higher in comparison to NSMs (where two CCSNe are required in order to form the two NSs). This potentially allows them to boost the abundances in terms of [Eu/Fe] much stronger than NSMs can. As can be seen in Section 4.3, the number of BHNSMs is higher in the beginning and subsequently lowers substantially. This leads to a decrease in the abundance boost and hence to less scatter in [Eu/Fe] abundances at higher metallicities.

Furthermore, if the mass range of failed supernovae in the IMF increases for lower metallicities, the event rate of BHNSMs increases accordingly and thus their nucleosynthetic influence towards low metallicities increases. This will be discussed in Section 4.3.

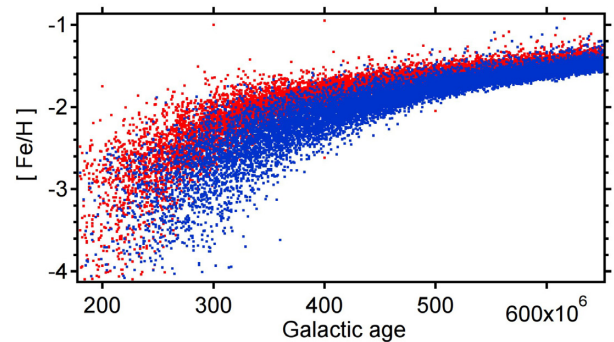


Figure 3. Illustration of a shifted age–metallicity relation. Blue (red) squares represent model stars in a model that does (not) permit failed SNe. A model that permits failed SNe produces less Fe per time step, so the [Fe/H] enrichment is delayed in comparison to a model that does not allow failed SNe.

4.2 Age–metallicity relation

In a model where no failed SNe are allowed, all HMSs die in a CCSN. So, all HMSs eject Fe at the end of their life, and contribute it to the Galactic Fe inventory. Opposed to that, a model where failed SNe are allowed, some stars collapse into a BH. This means that those stars do not contribute to the Galactic Fe. If the same star formation rate for both of these models is assumed, a model permitting failed SNe has thus less CCSN events per time step compared to a model where all stars die in a CCSN. This leads to a slower increase in [Fe/H] versus time. This also has implications on the GCE of r-process elements: All CBMs have a coalescence time between the death of the two stars and the merger event. When (in a model with enabled failed SNe) the [Fe/H] enrichment is slowed down with respect to time, the coalescence time-scale of CBMs is of less importance. In other words, less nearby CCSNs occur during the coalescence time. This allows CBM products to be ejected into a region that is less Fe rich than in a comparable model with no failed SNe permitted. See Fig. 3 for illustration.

4.3 The dominant r-process site

Since in this simulation *individual* stars and nucleosynthesis sites are followed, we can keep track of the number of individual events per time step. This allows us to determine which site (BHNSMs or NSM) is the *dominant* site contributing to the r-process element production throughout the history of the Galaxy. Since NSMs seem to be the dominant site (≥ 50 per cent of all CBM events at all times), we consider the relative importance of BHNSMs with respect to overall CBMs (=BHNSMs + NSMs) in Fig. 4. While the first r-process production events at early Galactic stages seem to be approximately equally performed by both types of CBMs, this changes rapidly towards NSMs as dominant r-process site. Already in early Galactic evolution stages ($t \geq 400$ My), the relative importance of BHNSMs in respect to all CBMs has reached its final value of ≈ 10 per cent of all CBMs. This originates in the fact that a large portion of stars (all stars $m \geq 30 M_{\odot}$) at lower metallicity ($[\text{Fe}/\text{H}] \leq -2$) will end up as a BH, while at higher metallicities only the stars in the range $22.8 M_{\odot} \leq m \leq 25.6 M_{\odot}$ will end up as BHs, according to the PUSH calculations utilized here.

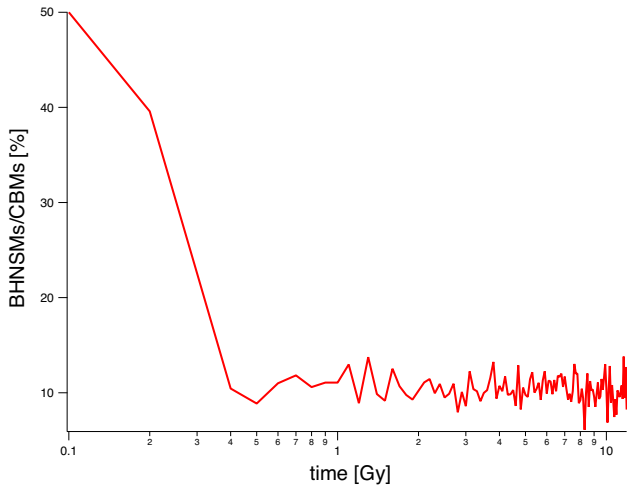


Figure 4. Relative occurrence of BHNSMs with respect to all CBMs (BHNSMs + NSMs) using a model where stars $\geq 30 M_{\odot}$ at lower metallicity ($Z \leq 10^{-2} Z_{\odot}$), and stars $22.8 M_{\odot} \leq m \leq 25.6 M_{\odot}$ at higher metallicity die in a failed SN instead of a CCSN.

5 CONCLUSIONS AND DISCUSSION

In this work, we have shown that the two major issues of the GCE of *r*-process elements, namely (a) the large scatter in abundances in comparison to alpha-elements at lower metallicities and (b) that *r*-process elements are abundant at low metallicities, can be explained in our GCE model by including BHNSMs as a second *r*-process element production site in addition to NSMs.

This scenario is complementary to magnetorotational supernovae, or even collapsars, related to single stars and their early appearance in Galactic evolution, but this study shows that BHNSMs could already produce the required effect.

The main advantage of BHNSMs acting as a second *r*-process site is that, contrary to NSMs, only *one* NS (plus one BH) is required to perform an *r*-process event. Hence only *one* previous successful CCSN is required, so the surrounding ISM is only polluted by Fe *once* as opposed to *twice* for NSMs. This advantage permits that BHNSMs occur in environments with less Fe content than the environment of NSMs. A second advantageous effect is that due to a higher failed SN rate at lower metallicities, i.e. less Fe-producing CCSNe, the overall enhancement of $[\text{Fe}/\text{H}]$ is progressing slower in time, reducing the significance of the coalescence time-scales of CBM.

Furthermore, we have shown that, despite that at early Galactic stages the *r*-process contribution of BHNSMs and NSMs to the Galactic *r*-process content is comparable, the contribution of NSMs is dominant over BHNSMs at later Galactic stages. This can be explained by more successful CCSN explosions with respect to failed SN explosion compared to lower metallicities, leading to a larger number of NSMs than BHNSMs.

There remain a number of open questions in this work, related to the stochastic nature of this GCE approach (as already addressed in Wehmeyer et al. 2015), as well as the specific implementation utilized this work.

(i) We did not include CCSNe as *r*-process element sources, although there might be a chance for a small contribution to the abundance of *r*-process elements or a contribution to the ‘weak’ *r*-process by CCSNe.

(ii) Also, we did not include the contribution of sub-haloes (such as dwarf galaxies) to the chemical enrichment of the Galaxy.

(iii) Furthermore, we did not include magnetorotational jet-supernovae or collapsars. They would have a similar, or even stronger (essentially emitting no Fe) effect, as described here for BHNSMs, but require strong assumptions on magnetic fields and stellar rotation, which would need to be confirmed observationally.

(iv) The predicted rates for CBMs required to explain the chemical evolution are arguably high. They are well at the upper end of the spectrum in comparison to similar GCE calculations as inferred by Côté et al. (2017). Still, these are in overall agreement with the LIGO detection rates.

(v) It has been shown by recent population synthesis studies (e.g. Dominik et al. 2012; Belczynski et al. 2017; Chruslinska et al. 2018) that parametrized delay time *distributions* (DTDs) should be used for CBMs instead of fixed coalescence time-scales. Thus, our approach oversimplifies the GCE of *r*-process elements in the metallicity region of $[\text{Fe}/\text{H}] \geq -1$, omitting the modelling difficulties associated with employing probably more realistic DTDs. See Côté et al. (2017, 2018) and Hotokezaka et al. (2018) for a discussion of this issue. A further effect, not yet considered here, could be that the coalescence time for massive binary systems containing one BH is possibly shorter than that for NSMs.

(vi) Since the direct swallowing of a NS by a BH probably leaves no *r*-process matter behind, we did not consider this case here. Hence, our predicted *r*-process element production rate in Section 3.2.4 omits this channel and thus has to be seen as a lower limit of a gravitational wave emission rate. However, this event would not alter the conclusions of Section 4.2, since the effect mentioned in that section originates only in the absence of Fe ejection by failed SNe (as opposed to successful Fe ejection in a case where *all* CCSNe eject Fe).

Future work towards the better understanding of the origin or the *r*-process elements will probably require

(i) Detailed predictions of the explodability of low-metallicity stars being employed in a GCE model instead of a parametrized approach.

(ii) The efforts taken in this work should be re-examined using CCSN explodability predictions of different groups, e.g. Ugliano et al. (2012), Ertl et al. (2016), and Sukhbold et al. (2016), and it should be examined whether this would change the required CBM event frequency, as well as the evolution of the BHNSMs/NSM ratio.

(iii) Future work should address the implications of CCSN kicks on the survival probability and dislocation of stellar binary systems (e.g. Belczynski & Bulik 1999): If a kick by a CCSN was strong enough to make the binary system leave the supernova remnant bubble, the succeeding CBM event might take place in an area of the Galaxy that has not been polluted by CCSN ejecta before. Such an event might even contribute *r*-process elements at even lower metallicities than the CBMs happening inside a CCSN bubble considered in this work.

(iv) Future work should include DTDs instead of fixed coalescence time-scales in this model.

(v) A future effort should be to include Jet-SNe as well as NSMs and BHNSMs as *r*-process element source. Of course, this would increase the level of complexity, since this would add another degree of freedom to the evolution of the Galaxy.

(vi) The next LIGO/Virgo run will probably provide us with a more accurate rate of CBMs. As soon as those are available, refined GCE calculations should be performed using these improved rates.

ACKNOWLEDGEMENTS

We thank Maria Lugaro, Chiaki Kobayashi, Albino Perego, Raphael Hirschi, Stephan Rosswog, Tim Beers, C. Gareth Few, and Brad K. Gibson for fruitful discussions. We further extend our gratitude to Sanjana Curtis and Kevin Ebinger who have provided us with the PUSH predictions that play a crucial role for the considerations in this study.

BW is supported by a fellowship of the Swiss National Science Foundation (SNF). BW and CF acknowledge support from the Research Corporation for Science Advancement through a Cottrell Scholar Award. CF was partially supported by the United States Department of Energy, Office of Science, Office of Nuclear Physics (award numbers SC0010263 and DE-FG02-02ER41216). FKT was supported by the European Research Council (FP7) under ERC Advanced Grant Agreement No. 321263 - FISH, and the SNF. MP acknowledges the support from the SNF and the ‘Lendület-2014’ Programme of the Hungarian Academy of Sciences (Hungary), of STFC, through the University of Hull Consolidated Grant ST/R000840/1, and access to VIPER, the University of Hull High Performance Computing Facility. BW, BC and MP acknowledge the support from the ERC Consolidator Grant (Hungary) funding scheme (project RADIOSTAR, G.A. n. 724560). BW, CF, BC, and MP acknowledge support of the National Science Foundation (USA) under grant No. PHY-1430152 (JINA Center for the Evolution of the Elements). This article is based upon the work from the ‘ChETEC’ COST Action (CA16117), supported by COST (European Cooperation in Science and Technology).

REFERENCES

Abbott B. P. et al., 2017a, *Phys. Rev. Lett.*, 119, 161101
 Abbott B. P. et al., 2017b, *ApJ*, 848, L12
 Abbott B. P. et al., 2017c, *ApJ*, 848, L13
 Abbott B. P. et al., 2018a, preprint ([arXiv:1811.12907](https://arxiv.org/abs/1811.12907))
 Abbott B. P. et al., 2018b, preprint ([arXiv:1811.12940](https://arxiv.org/abs/1811.12940))
 Arcones A., Thielemann F.-K., 2013, *J. Phys. G: Nucl. Phys.*, 40, 013201
 Argast D., Samland M., Thielemann F.-K., Qian Y.-Z., 2004, *A&A*, 416, 997
 Arnould M., Goriely S., Takahashi K., 2007, *Phys. Rep.*, 450, 97
 Barklem P. S. et al., 2005, *A&A*, 439, 129
 Bauswein A., Goriely S., Janka H.-T., 2013, *ApJ*, 773, 78
 Beers T. C., Holmbeck E. M., Placco V. M., Hansen T. T., Simon J. D., Thompson I., Frebel A., Sakari C. M., 2018, *IAUS*, 334, 277B
 Belczynski K. et al., 2018, preprint ([arXiv:1706.07053v3](https://arxiv.org/abs/1706.07053v3))
 Belczynski K., Bulik T., 1999, *A&A*, 346, 91
 Biémont E., Karner C., Meyer G., Träger F., zu Putlitz G., 1982, *A&A*, 107, 166
 Bisterzo S., Travaglio C., Gallino R., Wiescher M., Käppeler F., 2014, *ApJ*, 787, 10
 Bravo E., Domínguez I., Badenes C., Piersanti L., Straniero O., 2010, *ApJ*, 711, L66
 Burris D. L., Pilachowski C. A., Armandroff T. E., Sneden C., Cowan J. J., Roe H., 2000, *ApJ*, 544, 302B
 Burrows A., 2013, *Rev. Mod. Phys.*, 85, 245.
 Burrows A., Vartanyan D., Dolence J. C., Skinner M. A., Radice D., 2018, *SSRv*, 214, 33
 Carr B., Kühnel F., Sandstad M., 2016, *PhRvD*, 1994, 83504
 Cescutti G., Romano D., Matteucci F., Chiappini C., Hirschi R., 2015, *A&A*, 577, 139

Charbonnel C., Meynet G., Maeder A., Schaller G., Schaerer D., 1993, *A&AS*, 101, 415C
 Chornock R. et al., 2017, *ApJ*, 848, 19
 Chruslinska M., Belczynski K., Klencki J., Benacquista M., 2018, *MNRAS*, 474, 2937
 Cohen J. G., Huang W., 2009, *ApJ*, 701, 1053
 Côté B. et al., 2019, *ApJ*, 875, 106
 Côté B., Belczynski K., Fryer C. L., Ritter Ch., Paul A., Wehmeyer B., O’Shea B. W., 2017, *ApJ*, 836, 230C
 Cowan J. J., Thielemann F.-K., Truran J. W., 1991, *Phys. Rep.*, 208, 267
 Cowan J. J., Sneden C., Lawler J. E., Aprahamian A., Wiescher M., Langanke K., Martinez-Pinedo G., Thielemann F.-K., 2019, preprint ([arXiv:1901.01410](https://arxiv.org/abs/1901.01410))
 Cowperthwaite P. S. et al., 2017, *ApJ*, 848, 10
 Curtis S., Ebinger K., Fröhlich C., Hempel M., Perego A., Liebendörfer M., Thielemann F.-K., 2019, *ApJ*, 870, 2
 Dominik M., Belczynski K., Fryer C., Holz D. E., Berti E., Bulik T., Mandel I., O’Shaughnessy R., 2012, *ApJ*, 759, 52
 Duchêne G., Kraus A., 2013, *ARA&A*, 51, 269
 Ebinger K., 2017, PhD thesis, edoc.unibas.ch
 Ebinger K., Curtis S., Fröhlich C., Hempel M., Perego A., Liebendörfer M., Thielemann F.-K., 2019, *ApJ*, 870, 1
 Eichler M. et al., 2015, *ApJ*, 808, 30E
 Eichler D., Livio M., Piran T., Schramm D. N., 1989, *Nature*, 340, 126
 Ertl T., Janka H.-Th., Woosley S. E., Sukhbold T., Ugliano M., 2016, *ApJ*, 818, 124
 François P. et al., 2007, *A&A*, 476, 935
 Frebel A., 2018, *Ann. Rev. Nucl. Part. Sci.*, 68, 237
 Freiburghaus C., Rosswog S., Thielemann F.-K., 1999, *ApJ*, 525, L121
 Fröhlich C. et al., 2006, *ApJ*, 637, 415
 Fröhlich C., Martinez-Pinedo G., Liebendörfer M., Thielemann F.-K., Bravo E., Hix W., Langanke K., Zinner N., 2006, *PRL*, 96, 142502
 Fujimoto S., Hashimoto M., Kotake K., Yamada S., 2006, *Origin Matter Evol. Galaxies*, 847, 386
 Fujimoto S., Nishimura N., Hashimoto M., 2008, *ApJ*, 680, 1350
 Garcia-Bellido J., 2018, PoS(EDSU2018) 042. Proc. Sci., Trieste, Italy
 Garcia-Bellido J., Linde A. D., Wands D., 1996, *Phys. Rev. D*, 54, 6040
 Geisler D., Smith V. V., Wallerstein G., Gonzalez G., Charbonnel C., 2005, *AJ*, 129, 1428
 Gompertz B. P. et al., 2018, *ApJ*, 860, 62G
 Greggio L., 2005, *A&A*, 441, 1055
 Halevi G., Mösta P., 2018, *MNRAS*, 477, 2366
 Hansen T. T. et al., 2018, *ApJ*, 858, 92H
 Haynes C. J., Kobayashi C., 2019, *MNRAS*, 483, 5123
 Heger A., Fryer C. L., Woosley S. E., Langer N., Hartmann D. H., 2003, *ApJ*, 591, 288H
 Hinderer T. et al., 2018, preprint ([arXiv:1808.03836](https://arxiv.org/abs/1808.03836))
 Hirai Y., Ishimaru Y., Saitoh T. R., Fujii M. S., Hidaka J., Kajino T., 2015, *ApJ*, 814, 41
 Hirschi R., 2007, *A&A*, 461, 571
 Hirschi R., Meynet G., Maeder A., 2005, *A&A*, 443, 581
 Horowitz C. J. et al., 2018, preprint ([arXiv:1805.04637](https://arxiv.org/abs/1805.04637))
 Hotokezaka K., Beniamini P., Piran T., 2018, *J. Mod. Phys. D*, 27, 1842005
 Ishimaru Y., Wanajo S., Prantzos N., 2015, *ApJ*, 804L, 35I
 Iwamoto K., Brachwitz F., Nomoto K., Kishimoto N., Umeda H., Hix W. R., Thielemann F.-K., 1999, *ApJS*, 125, 439
 Janka H.-T., 2017, in *Handbook of Supernovae*. Springer International Publishing, Basel-Stadt, Switzerland
 Janka H.-T., Melson T., Summa A., 2016, *Ann. Rev. Nucl. Part. Sci.*, 66, 341
 Ji A. P., Frebel A., Chiti A., Simon J. D., 2016, *Nature*, 531, 610
 Jones S. et al., 2013, *ApJ*, 772, 150J
 Just O., Bauswein A., Pulpillo R. A., Goriely S., Janka H.-T., 2015, *MNRAS*, 448, 541
 Kalogera V. et al., 2004, *ApJ*, 601, L179
 Käppeler F., Gallino R., Bisterzo S., Aoki W., 2011, *RvMP*, 83, 157

- Kasen D., Metzger B., Barnes J., Quataert E., Ramirez-Ruiz E., 2017, *Nature*, 51, 80K
- Kennicutt R. C., Jr, 1998, *ApJ*, 498, 541
- Kirby E. N., Cohen J. G., Guhathakurta P., Cheng L., Bullock J. S., Gallazzi A., 2013, *ApJ*, 779, 102
- Kobayashi C., Nakasato N., 2011, *ApJ*, 729, 16K
- Komiya Y., Shigeyama T., 2016, *ApJ*, 830, 76
- Korobkin O., Rosswog S., Arcones A., Winteler C., 2012, *MNRAS*, 426, 1940
- Larson R., 1991, *ASPC*, 20, 571L
- Lattimer J. M., Schramm D. N., 1974, *ApJ*, 192, L145
- Letarte B., Hill V., Tolstoy E., Jablonka P., Shetrone M. et al., 2010, *A&A*, 523, A17
- Leung S. C., Nomoto K., 2018, *ApJ*, 861, 143
- Liebigdorfer M., Mezzacappa A., Messer O. E. B., Martinez-Pinedo G., Hix W. R., Thielemann F.-K., 2003, *Nucl. Phys. A*, 719, C144
- Limongi M., Chieffi A., 2006a, *New Astron. Rev.*, 50, 474
- Limongi M., Chieffi A., 2006b, *ApJ*, 647, 483
- Limongi M., Chieffi A., 2018, *ApJS*, 237, 13
- Marshall J. et al., 2018, preprint ([arXiv:1812.01022](https://arxiv.org/abs/1812.01022))
- Matteucci F., Greggio L., 1986, *A&A*, 154, 279M
- Matteucci F., Romano D., Arcones A., Korobkin O., Rosswog S., 2014, *MNRAS*, 438, 2177
- McWilliam A., Wallerstein G., Mottini M., 2013, *ApJ*, 778, 149
- Mennekens N., Vanbeveren D., 2014, *A&A*, 564, A134
- Mösta P. et al., 2014, *ApJ*, 785, L29
- Mösta P., Ott Ch. D., Radice D., Roberts L. F., Schnetter E., Haas R., 2015, *Nature*, 528, 376M
- Muratov A. L., Kereš D., Faucher-Giguère C.-A., Hopkins P. F., Quataert E., Murray N., 2015, *MNRAS*, 454, 2691
- Nishimura N., Sawai H., Takiwaki T., Yamada S., Thielemann F.-K., 2017, *ApJ*, 836, L21
- Nomoto K., Kobayashi C., Tominaga N., 2013, *ARA&A*, 51, 457N
- O'Dell C. R., McCullough P. R., Meixner M., 2004, *AJ*, 128, 2339
- Obergaulinger M., Just O., Aloy M. A., 2018, *J. Phys. G Nuc. Phys.*, 45, 084001
- Ojima T., Ishimaru Y., Wanajo S., Prantzos N., François P., 2018, *ApJ*, 865, 87
- Paczynski B., 1986, *ApJ*, 308, L43
- Panov I. V., Korneev I. Yu., Thielemann F.-K., 2008, *AL*, 34, 189
- Perego A., Hempel M., Fröhlich C., Ebinger K., Eichler M., Casanova J., Liebendörfer M., Thielemann F.-K., 2015, *ApJ*, 806, 275
- Pillepich A. et al., 2018, *MNRAS*, 473, 4077
- Pruet J., Woosley S. E., Buras R., Janka H.-T., Hoffman R. D., 2005, *ApJ*, 623, 325
- Pruet J., Hoffman R. D., Woosley S. E., Janka H.-T., Buras R., 2006, *ApJ*, 644, 1028
- Reed D. S., Balick B., Hajian A. R., Klayton T. L., Giovanardi S., Casertano S., Panagia N., Terzian Y., 1999, *ApJ*, 118, 2430
- Rembiasz T., Guilet J., Obergaulinger M., Cerdá-Durán P., Aloy M. A., Müller E., 2016, *MNRAS*, 460, 3316R
- Roederer I. U., Preston G. W., Thompson I. B., Shtetman S. A., Sneden C., 2014a, *ApJ*, 784, 158
- Roederer I. U., Preston G. W., Thompson I. B., Shtetman S. A., Sneden C., Burley G. S., Kelson G. G., 2014b, *AJ*, 147, 136
- Roederer I. U., Cowan J. J., Preston G. W., Shtetman S. A., Sneden C., Thompson I. B., 2014c, *MNRAS*, 445, 2970
- Roederer I. U. et al., 2010, *ApJ*, 724, 975R
- Rosswog S., 2013, *Phil. Trans. R. Soc. A*, 20120272,
- Rosswog S., 2015, *Living Rev. Comp. Astrophysics*, 1, 109
- Rosswog S., Korobkin O., Arcones A., Thielemann F.-K., Piran T., 2014, *MNRAS*, 439, 744
- Rosswog S., Sollerman J., Feindt U., Goobar A., Korobkin O., Wollaeger R., Fremling C., Kasliwal M. M., 2018, *A&A*, 615, 132R
- Ryan S. G., Aoki W., Norris J. E., Beers T. C., 2005, *ApJ*, 635, 349R
- Sawai H., Yamada S., 2016, *ApJ*, 817, 153S
- Schaerer D., Meynet G., Maeder A., Schaller G., 1993a, *A&AS*, 98, 523S
- Schaerer D., Charbonnel C., Meynet G., Maeder A., Schaller G., 1993b, *A&AS*, 102, 339S
- Schaller G., Schaerer D., Meynet G., Maeder A., 1992, *A&AS*, 96, 269S
- Schmidt M., 1959, *ApJ*, 121, 161
- Seitenzahl I. R. et al., 2013, *MNRAS*, 429, 1156
- Shen S., Cooke R. J., Ramirez-Ruiz E., Madau P., Mayer L., Guedes J., 2015, *ApJ*, 807, 115
- Shetrone M., Côté P., Stetson P. B., 2001, *PASP*, 113, 1122
- Shetrone M., Venn K. A., Tolstoy E., Primas F., Hill V., Kaufer A., 2003, *AJ*, 125, 684
- Siegel D. M., Barnes J., Metzger B. D., 2019, *Nature*, 569, 241
- Simmerer J., Sneden C., Cowan J. J., Collier J., Woolf M., Lawler J. E., 2004, *ApJ*, 617, 1091
- Sneden C., Cowan J. J., Gallino R., 2008, *ARA&A*, 46, 241
- Starkenburger E. et al., 2013, *A&A*, 549, 88
- Suda T. et al., 2008, *PASJ*, 60, 1159
- Suda T., Yamada S., Katsuta Y., Komiya Y., Ishizuka C., Aoki W., Fujimoto M. Y., 2011, *MNRAS*, 412, 843
- Sukhbold T., Ertl T., Woosley S. E., Brown J. M., Janka H.-T., 2016, *ApJ*, 821, 38S
- Takahashi K., Witt J., Janka H. T., 1994, *A&A*, 286, 857
- Tanaka M. et al., 2017, *PASJ*, 69, 102
- Tanvir N. R. et al., 2017, *ApJ*, 848, 27
- Tauris T. M. et al., 2017, *ApJ*, 846, 170T
- Thielemann F.-K., 2015, *Nat. Phys.*, 11, 993
- Thielemann F.-K., Brachwitz F., Höflich P., Martinez-Pinedo G., Nomoto K., 2004, *New Astron. Rev.*, 48, 605
- Thielemann F.-K. et al., 2011, *Progr. Part. Nucl. Phys.*, 66, 346
- Thielemann F.-K., 2018, preprint ([arXiv:1809.07187](https://arxiv.org/abs/1809.07187))
- Thielemann F.-K., Eichler M., Panov I. V., Wehmeyer B., 2017, *Ann. Rev. Nuc. Part. Sci.*, 67, 253
- Timmes F. X., Brown E. F., Truran J. W., 2003, *ApJ*, 590, L83
- Travaglio C., Hillebrandt W., Reinecke M., 2005, *A&A*, 443, 1007
- Ugolino M., Janka H.-Th., Marek A., Arcones A., 2012, *ApJ*, 757, 1
- van de Voort F., Quataert E., Hopkins P. F., Keres D., Faucher-Giguere C.-A., 2015, *MNRAS*, 447, 140
- Villar V. A. et al., 2017, *ApJ*, 851, 12
- Wanajo S., 2006, *ApJ*, 647, 1323W
- Wanajo S., 2013, *ApJ*, 770, L22
- Wanajo S., Sekiguchi Y., Nishimura N., Kiuchi K., Kyutoku K., Shibata M., 2014, *ApJ*, 789, L39
- Wang H. et al., 2017, *ApJ*, 851, L18
- Wehmeyer B., Pignatari M., Thielemann F.-K., 2015, *MNRAS*, 452, 1970
- Winteler C., Käppeli R., Perego A., Arcones A., Vasset N., Nishimura N., Liebendörfer M., Thielemann F.-K., 2012, *ApJ*, 750, L22
- Wollaeger R. T. et al., 2018, *MNRAS*, 478, 3298
- Woosley S. E., Heger A., 2007, *PhR*, 442, 269
- Woosley S. E., Wilson J. R., Mathews G. J., Hoffman R. D., Meyer B. S., 1994, *ApJ*, 433, 229
- Woosley S. E., Heger A., Weaver T. A., 2002, *RvMP*, 74, 1015
- Yamada S., Suda T., Komiya Y., Aoki W., Fujimoto M. Y., 2013, *MNRAS*, 436, 1362

This paper has been typeset from a \LaTeX file prepared by the author.